Engineering Analysis with Boundary Elements 177 (2025) 106259

Contents lists available at ScienceDirect

Engineering Analysis with Boundary Elements

journal homepage: www.elsevier.com/locate/enganabound

Indentation of axisymmetric rigid punch: Model implementation by a Python Algorithm

Krupal Patel [a,*], Etienne Barthel [b], Matteo Ciccotti [b]

[a] Department of Engineering Science, University of Oxford, OX1 3PJ, Oxford, United Kingdom
[b] Soft Matter Sciences and Engineering Lab, ESPCI Paris, PSL University, CNRS, Sorbonne Université, 75005 Paris, France

ARTICLE INFO

Keywords:
Finite element method
Boundary element method
Poker-chip test

ABSTRACT

We present a computationally efficient Python algorithm based on the Boundary Element Method (BEM) for frictionless linear elastic axisymmetric contact of coated solids. The algorithm solves indentation problems using conical, spherical, and cylindrical flat indenters, with results also reported for flat punch indentation on a soft-coated substrate. To validate BEM, we implement Finite Element Method (FEM) simulations, analyzing soft layers with Poisson ratios of 0.25, 0.4, and 0.49, aspect ratios from 0.25 to 10, and modulus mismatches of 10 and 100. BEM and FEM show good agreement for compressible soft layers but diverge as incompressibility increases. For Poisson's ratio of 0.4999, BEM fails due to confinement effects. We verify FEM results using the Poker-chip test, confirming accuracy in highly confined, nearly incompressible cases. For compressible soft layer and large aspect ratios, we found good agreement between BEM and analytical result of Poker-chip test applicable in that regime.

1. Introduction

The indentation of an axisymmetric punch on a coated substrate has generated significant interest in materials science and engineering due to its relevance in various industrial applications [1,2]. Coating substrate systems are commonly encountered in fields such as automotive, aerospace, and microelectronics, where the performance and durability of coated components are of utmost importance [3,4]. The indentation process simulates localized loading, mimicking real-world scenarios involving contact and deformation. Therefore, accurate modeling of this process is essential for predicting the mechanical response, optimizing coating designs, and ensuring structural integrity. Here we explore different numerical and analytical approaches employed to model the indentation of an axisymmetric punch on a coated substrate. Finite element analysis (FEA) is widely used to simulate the indentation process, considering the material properties, coating thickness, and substrate geometry. FEA provides valuable information on the stress and strain distribution, contact pressure, and deformation characteristics within the coating-substrate system. However, we employed FEA to validate the results given by the Boundary Element Method but it is time-consuming. In applications such as calculating the mechanical properties of solar panels, the cone indenter is useful. An indenter that is flat, cylindrical, or spherical can be used to mimic the elastic or visco-elastic properties of articular cartilage and polymeric films or functional coatings on hard substrates. This topic has been covered in many publications [5–10]. The issue becomes similar to that of a flat punch indenting into a flat elastic half-space when the indenter's radius a is substantially smaller than the layer's thickness t. Sneddon's solution can be used to get the corresponding load-depth relation [5]. Jaffar [7] and Yang [8] have given an asymptotic solution to the contact issue from which the load depth relation can be derived in the scenario when a is significantly greater than t. The development of analytical solutions appears to be unachievable for the large gap that still exists between Sneddon's solution and the asymptotic solution, indicating that the issue must be resolved numerically. Hayes et al. [9] gave explicit expressions of the load depth curve for Poisson ratios of 0.3–0.5 and a/t ratios in the range of 0.2–8 based on the method put forth by Lebedev and Ufliand [10]. Jaffar [7] proposed a simple numerical technique [6] that can be used to solve the problem when a/t ratio is in the range of 0 to 20.

There are a few other examples of thin film-related problems which are solved numerically. In work by Zhi-Hui Xu et al. [11], they utilized the finite element method to study the substrate effect on indentation behavior. They questioned the existence of universal critical penetration after which substrate effect sets in. The critical penetration depth is dependent on many other parameters. The elastic–plastic axisymmetric contact between a rigid ball and TiN coatings of varying thickness on various substrates has been simulated using the finite element

* Corresponding author.
E-mail addresses: krupalpatel12@hotmail.com (K. Patel), etienne.barthel@espci.fr (E. Barthel), matteo.ciccotti@espci.fr (M. Ciccotti).

https://doi.org/10.1016/j.enganabound.2025.106259
Received 22 January 2025; Received in revised form 3 April 2025; Accepted 4 April 2025
Available online 26 April 2025
0955-7997/© 2025 The Authors. Published by Elsevier Ltd. This is an open access article under the CC BY license (http://creativecommons.org/licenses/by/4.0/).

method by Y.Sun et al. [12], while C.C. Lee et al. [13] employed a fracture-based finite element model of peeling to study multilayered active-matrix organic light-emitting diode (AMOLED) architecture. In this work, they analyzed the adhesive behavior of the polyimide /debonding layer (DBL) interface via the utilization of the modified virtual crack closure technique. In multilayered active-matrix organic light-emitting diode (AMOLED) architecture, the interfacial adhesive strength is a crucial factor to take into account because it affects the mechanical reliability issue caused by challenging organic/inorganic hybrid lamination and final debonding. To determine the contact stresses in elastic double-layer systems under a typical pressure distribution, like that present in the Hertzian contact between a spherical indenter and an elastic half-space, H. Djabella et al. [14] used the finite element approach. S. Zak et al. [15] also used FEM to show the difference between elastic and plastic field in indentation of coated system. A. Lassnig at al. [16] extended this approach to multilayered system. S. Zak [17] used FEM to show the effect of tip sharpness on the strain field under the indenter. Moreover, Q. Li et al. [18] gave new formulation of boundary element method for simulating the nonadhesive and adhesive contact between an indenter of arbitrary shape and an elastic half-space coated with an elastic layer of different material which is based on the Fast Fourier Transform.

Boussinesq [19] first considered the problem of determining the stress distribution within the elastic half-space when a rigid punch deforms it. The form of his solution was not helpful for practical computations and partial numerical results based on his solution were derived in the case of conical [20] and flat [21] indenters by A.E.H. Love. An important protagonist in developing a simpler solution methodology to Boussinesq's problem (i.e. punch indenting on elastic homogeneous half-space) is I. N. Sneddon [5], who used the Hankel transform and dual integral technique. Li et al. [22] presented the elastic solution of a coated half-space with perfect interfacial bonding under an axisymmetrical compressive loading on the plane surface. It is particularly useful to model the nano-indentation of thin-film coating/substrate systems. H.J. Gao et al. [23] studied the contact problem of a rigid cylindrical punch indenting a layered elastic half-space. They used the moduli-perturbation method to derive the first-order accurate analytical solution for the contact compliance of a nonhomogeneous medium with layered or continuously varying moduli in the depthwise direction. A.-S. Huguet et al. [24] suggest a synthetic solution to the issue of the adhesive contact of axisymmetric elastic bodies. Thus, a practical and all-encompassing formulation is created, which is proven to immediately give the majority of usable models. Based on the systematic approach by Huguet et al. [24], E. Barthel et al. [25] proposed an algorithm that can efficiently handle the problem of spherical punch contact to coated elastic half-space which is based on the Boundary Element Method. A. Perriot and E. Barthel [26] have developed an algorithm based on the punch (i.e. conical, flat cylindrical, and parabolic) indentation to the coated elastic half-space using Boundary Element Method. YY. Lin et al. [27] have shown the analytic expressions for the stresses away from the edges, and the effect of lateral constraint in the case of Poker-chip configuration of the Flat Punch (Tack) Test for Pressure-Sensitive Adhesives.

In earlier work [25], A. Perriot and E. Barthel gave the simple algorithm and some representative examples. Here, we would focus on a Python algorithm based on previous work [25] and how we can use it in practice. We report some results in terms of contact stiffness of the system of flat punch indenting coated substrate as well as the local response of the system close to the boundary of the flat punch in terms of stress intensity factor [28]. In addition to that, we investigate some limit cases where the modeling breaks down while solving the problem of flat punch indentation to the coated half-space.

2. Methodology

We start with the simple problem when the thickness of the soft layer sandwiched between the two stiff materials is infinite or in other words the problem of the flat punch indention on the homogeneous half-space as we know the analytical solution for the stiffness and the stress intensity factor [28] in this case as per Eqs. (1) and (2) respectively.

$$S_0 = 2aE_1^* \tag{1}$$

$$K_0 = \frac{E_1^* \delta_{fp}}{\sqrt{\pi a}} \tag{2}$$

To solve the more difficult problem of flat punch indentation to the coated elastic half-space, A. Perriot and E. Barthel [26] have developed an algorithm using the Boundary Element method with the help of Green's function. Let us consider the system of coated elastic half-space under a load of an axisymmetric frictionless indenter as shown in Fig. 1(a). As per Fig. 1(a), the soft layer has the thickness t, the punch has radius a and the substrate is as usual semi-infinite. The layer and the substrate have perfect adhesion and are elastic, isotropic, and homogeneous. From Fig. 1(a), it is evident that E_0 and ν_0 are elastic moduli and the Poisson ratio of the substrate and similarly, E_1 and ν_1 are elastic moduli and the Poisson ratio of the layer. This is a mixed boundary value problem as one only knows the surface displacement under the contact and the applied stress outside of it. The boundary conditions of this problem are the following:

$$\begin{cases} \forall r \le a, & u_z(r) = \delta - p(r) \\ \forall r \ge a, & \sigma_z(r) = 0 \end{cases} \tag{3}$$

where $p(r)$ the shape of the indenter, a the contact radius and δ is the displacement.

For this problem, the equilibrium equation is given by a convenient form as per follow:

$$u_z(r) = \int_0^\infty dk \bar{\sigma_z}(k) J_0(kr) C(kt) \tag{4}$$

where,

$$C(kt) = \frac{2}{{E_1}^*} \frac{1 + 4b\,kt\,e^{-2kt} - ab\,e^{-4kt}}{1 - (a + b + 4b(kt)^2)e^{-2kt} + ab\,e^{-4kt}} \tag{5}$$

where,

$$a = \frac{\alpha\gamma_3 - \gamma_1}{1 + \alpha\gamma_3}, b = \frac{\alpha - 1}{\alpha + \gamma_1}, \alpha = \frac{E_1(1 + \nu_0)}{E_0(1 + \nu_1)}, \gamma_1 = 3 - 4\nu_1, \gamma_3 = 3 - 4\nu_0 \tag{6}$$

Here, $E_1^* = \frac{E_1}{1 - \nu_1^2}$, k is the wave vector and $J_0(x)$ is the 0th order Bessel function of the first kind. $\bar{\sigma_z}$ is the 0th order Hankel transform of σ_z defined as:

$$\bar{\sigma_z}(k) = \int_0^\infty dr r J_0(kr) \sigma_z(k) \tag{7}$$

We introduce the auxiliary fields g and θ defined as the cosine transforms of $\bar{\sigma}_z(r)$ and $k\,\bar{u}_z(r)$ respectively :

$$g(s) = \int_0^\infty dk\, \bar{\sigma}_z(k) \cos(ks) \tag{8}$$

$$\theta(s) = \int_0^\infty dk\, k\, \bar{u}_z(k) \cos(ks) \tag{9}$$

Expressing Eqs. (8) and (9) in the real space, we obtain:

$$g(s) = \int_s^\infty dr \frac{r\sigma_z(r)}{\sqrt{r^2 - s^2}} \tag{10}$$

$$\theta(s) = \frac{d}{ds} \int_0^s dr \frac{r u_z(r)}{\sqrt{s^2 - r^2}} \tag{11}$$

Rewriting Eq. (4) with the Hankel transform, we obtain the simple form:

$$k\bar{u}(k) = C(kt)\bar{\sigma_z}(k) \tag{12}$$

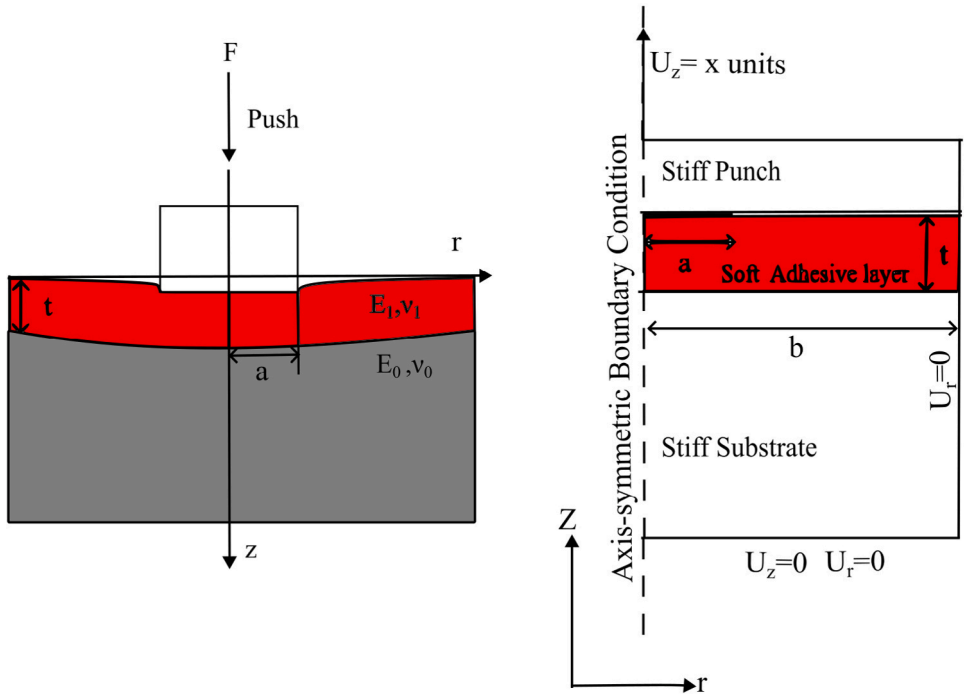

(a) Flat punch contact to the coated half-space (b) Geometry and Boundary conditions used in ABAQUS

Fig. 1. Flat punch contact to the coated substrate problem representation.

Note that $g(r) = 0$ for $r > a$. Apply cosine Fourier transform to Eq. (12) and we obtain the following equation after some simplification:

$$\theta(s) = \frac{2}{\pi}\int_0^a g(r)\left(\int_0^\infty dk\, C(kt)\cos(kr)\cos(ks)\right)dr \tag{13}$$

Then, under the contact, our indentation problem turns into an integral equation of the type $p(r) = \int_0^a f(s)M(r,s)\mathrm{ds}$ where p and M are known.

$$M(r,s) = \int_0^\infty dk\, C(kt)\cos(kr)\cos(ks) \tag{14}$$

To calculate integral M(r,s) in Eq. (14), Fast Fourier Transform is used. To evaluate the value of the integral equation $p(r) = \int_0^a f(s)M(r,s)\mathrm{ds}$, we used the trapezoidal rule. Hence, we solve the integral equation numerically by inverting the M(r,s). For normalization of the problem and numerical consideration, we give a detailed explanation in Appendix B. In addition to that we give a brief explanation about variables used in the code and how to get the converged solutions. The Python code is in Appendix A

To validate the Python code, we used FEM. We can refer to the same Fig. 1(a) as that of BEM. We compare the stiffnesses and the stress intensity factor in the case of BEM and FEM calculations. The primary purpose of this exercise is to validate the BEM calculations. We have decided to keep the coated substrate part of the FEM calculations 10 mm in depth and 10 mm in radius. Geometry and boundary conditions are shown in Fig. 1(b). To calculate the stress intensity factor, we put the initial crack at the interface between the unindented part of the soft adhesive layer and the rigid punch in ABAQUS which means that at the interface, nodes are not connected as explained in Fig. 1(b). To tackle the singularity at the crack tip, a spiderweb type of mesh was employed. With such a mesh the J-integral can be calculated over the concentric paths surrounding the node defined as the crack tip. The J-integral value is taken on contour number 50. The approximate size of the mesh elements near the crack tip is 1 μm which is 0.1% of the punch size "a". When Poisson's ratio is close to 0.5, bulk modulus approaches infinity. Under nearly incompressible conditions, any small error in the predicted volumetric strain will appear as a large error in the hydrostatic pressure and subsequently in the stresses. This error will, in turn, also affect the displacement prediction since external loads are balanced by the stresses, and may result in displacements very much smaller than they should be for a given mesh. This is called locking or no convergence at all. To overcome these difficulties, a mixed displacement-pressure formulation was developed which is available in the form of hybrid elements in ABAQUS. Hence, the hybrid and reduced integration type elements (CAX4RH and CAX3H) are used to take care of Poisson's ratio which is close to 0.5 in the case of incompressible adhesive layer [29].

The Poker-chip test is a way to test the strength of elastomers. The schematic and boundary conditions for FEM simulation are given in Fig. 2. In this test, a relatively compliant elastomer of thickness t is sandwiched between two rigid substrates which are pulled apart. Here the elastomer is incompressible and confined between the two substrates (i.e. $a \gg t$). YY. Lin et al. [27] have shown the analytic expressions for the stresses away from the edges, and the effect of lateral constraint in the case of Poker-chip configuration of the Flat Punch (Tack) Test for Pressure-Sensitive Adhesives. Using this expression for the normal stress one can derive the vertical force.

The vertical force F acting on the soft layer is obtained by integrating the normal stress over the area of the soft layer and is found to be

$$F = 3\pi\mu\frac{\delta}{t}a^2\left(1+\frac{1}{2}\left(\frac{a}{t}\right)^2\right) \tag{15}$$

Integrating Eq. (15), we get the strain energy as per the following eqn.:

$$U_d = \frac{3}{2}\pi\mu\frac{\delta^2}{t}a^2\left(1+\frac{1}{2}\left(\frac{a}{t}\right)^2\right) \tag{16}$$

From strain energy, one can derive the energy release rate:

$$J = \frac{1}{2\pi a}\frac{\partial U_d}{\partial a} \tag{17}$$

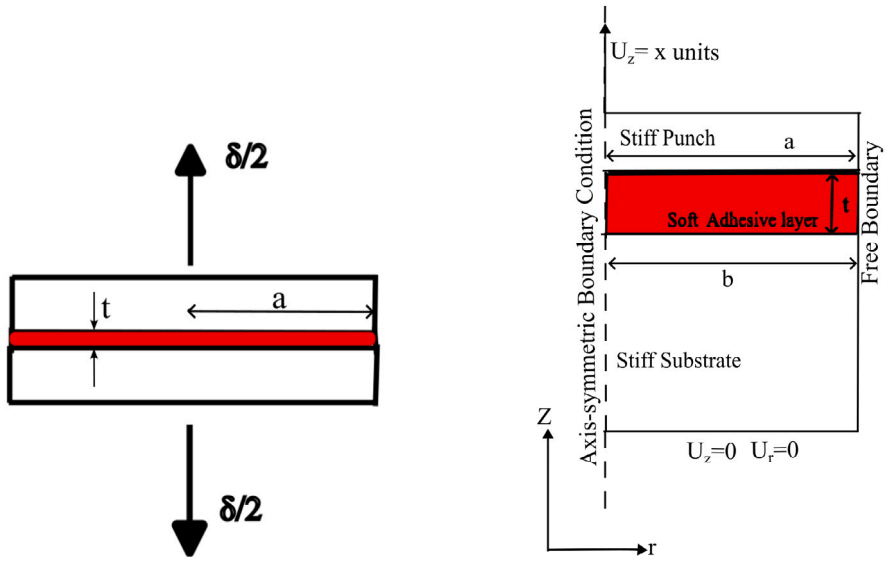

(a) Poker-chip test schematics (b) FEM: Boundary conditions for Pokerchip test

Fig. 2. Poker-chip test.

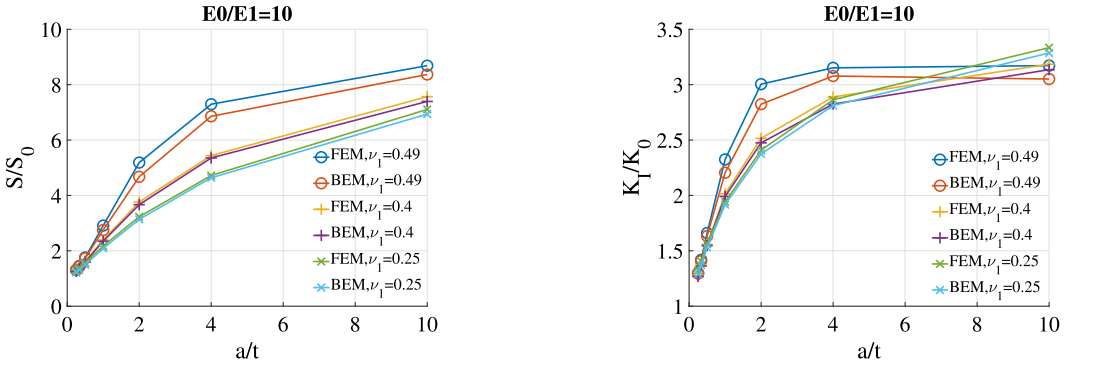

(a) Normalised Contact Stiffness (S/S_0) (b) Normalised Stress Intensity Factor (K_I/K_0)

Fig. 3. Comparison of contact properties calculated with the BEM and the FEM methods: Moduli Mismatch ratio 10:1, Poisson Ratio $\nu_1 = 0.49, 0.4, 0.25$, $\delta = 0.001$ mm, $a = 1$ mm while t is varying.

$$= \frac{3}{2}\mu\frac{\delta^2}{t}\left(1+\left(\frac{a}{t}\right)^2\right) \tag{18}$$

However, Eq. (15) is valid only when soft layer is incompressible. When soft layer is compressible and a/t ratio is very large there is another expression for measuring force which is given by Eq. (19)

$$F = 2\pi\mu\frac{\delta}{t}a^2\left(\frac{1-\nu_1}{1-2\nu_1}\right) \tag{19}$$

3. Results and discussion

To portray the usefulness of our Python algorithm based on the Boundary Element method, we first choose the case where the modulus mismatch ratio between substrate and soft layer is 10 as per Fig. 3. In Fig. 3(a), the contact stiffness is plotted against the aspect ratio while Fig. 3(b) showcases the stress intensity factor varying with the aspect ratio. It can be inferred from Fig. 3 that there is a very good agreement between BEM and FEM for both the contact stiffness and the stress intensity for the layer's poison ratios 0.25 and 0.4 and for the given range of aspect ratio. When soft layer becomes incompressible (i.e. ν_1 = 0.49), BEM method deviates from FEM for aspect ratios more than 1. We also show the convergence test for the BEM result in Appendix B. In the case of the finite element method, we checked the effect of increasing the substrate domain size by a factor of 2. However, we report the same contact stiffness even after increasing the substrate domain by a factor of 2. Hence, the choice of initial coated substrate domain size (R10 mm × H10 mm) is a wise choice for these sets of FEM simulations. Hence, we can use the Python algorithm and save computation time for practical cases where the Poisson's ratio of soft

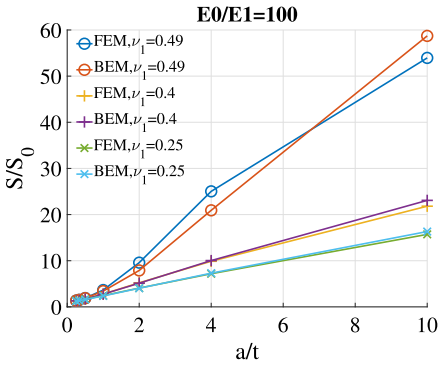

(a) Normalised Contact Stiffness (S/S_0)

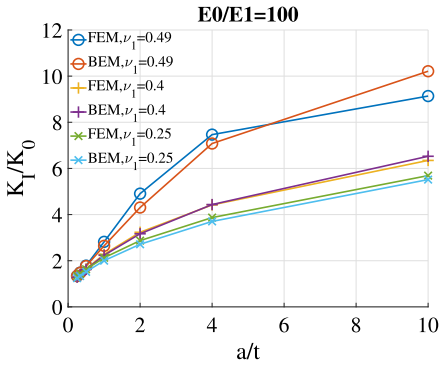

(b) Normalised Stress Intensity Factor (K_I/K_0)

Fig. 4. Comparison of contact properties calculated with the BEM and the FEM methods: Moduli Mismatch ratio 100:1, Poisson Ratio $\nu_1 = 0.49, 0.4, 0.25$, $\delta = 0.001$ mm, $a = 1$ mm while t is varying.

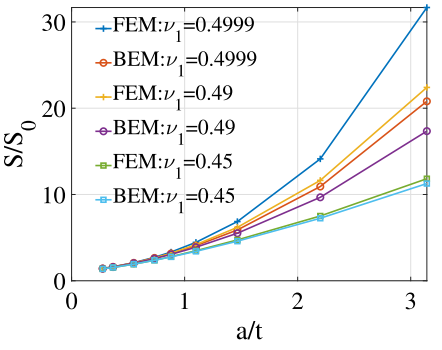

(a) Normalised contact stiffness (S/S_0)

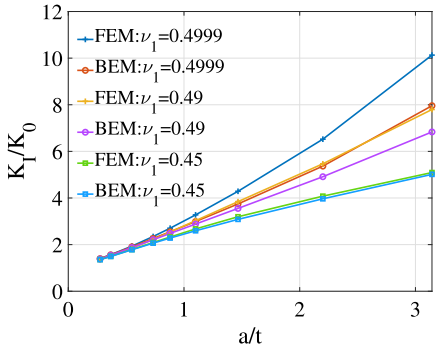

(b) Normalised Stress Intensity Factor (K_I/K_0)

Fig. 5. Impact of soft layer's Poisson ratio change on the normalized contact stiffness and the normalized stress intensity factor: Modulus mismatch 1000:1, $a = 1.1$ mm while t is varying.

layer is less than equal to 0.4. This is due to a particular feature of the boundary element method in which we use Green's function, and we need not to simulate the domain of infinite substrate as in the case of FEM. In other words, we can save computational time by using BEM.

It is evident from Fig. 4 that our Python algorithm based on BEM works very well even if we increase the modulus mismatch ratio to 100 and until the soft layer poison ratio in the range of 0.4 as it is in good agreement with FEM for reported aspect ratios. However, there is a discrepancy between BEM and FEM at $\nu_1 = 0.49$ at aspect ratios greater than 1.

From Fig. 5, we try to understand the effect of confinement and Poisson ratio on the domain of validity of our Python code. As we increase the confinement (i.e. $a/t \gg 1$), the mismatch between FEM and BEM result is evident at the elevated Poisson's ratio. In that regime, we discovered that the $C(kt)$ matrix is becoming singular for incompressible soft layer and at the elevated aspect ratios. Hence, it is difficult to invert the response function $C(kt)$. We have expanded the nominator and denominator of the $C(kt)$ function and found that when the soft layer is confined and becomes incompressible, the denominator is well-behaved while nominator goes to zero. Hence Green's function becomes singular. For more details regarding this, please visit Appendix C. Moreover, for FEM we need hybrid elements to tackle incompressibility but we do not have such provision in BEM.

On the other hand, in this particular regime, the Poker-chip test is useful to put forward the argument that FEM is doing a fine job in this regime at the elevated aspect ratio and highly incompressible soft layer having modulus of rigidity μ. In the FEM simulation, we tried to implement the same boundary conditions as that of the analytical results of the Poker-chip test. From Fig. 6(a), we found that the analytical results of the Poker-chip test and what we got by FEM are similar. Hence, we can deduce that if we change the boundary condition in the FEM simulation to match that of the Poker-chip test, we got a good agreement with the analytical expression of the Poker-chip test. It seems that the slope of the results given by the Poker-chip test parallels the FEM for the contact stiffness and the stress intensity factor when aspect ratio is more than 1. Hence, the FEM solution that is offset to

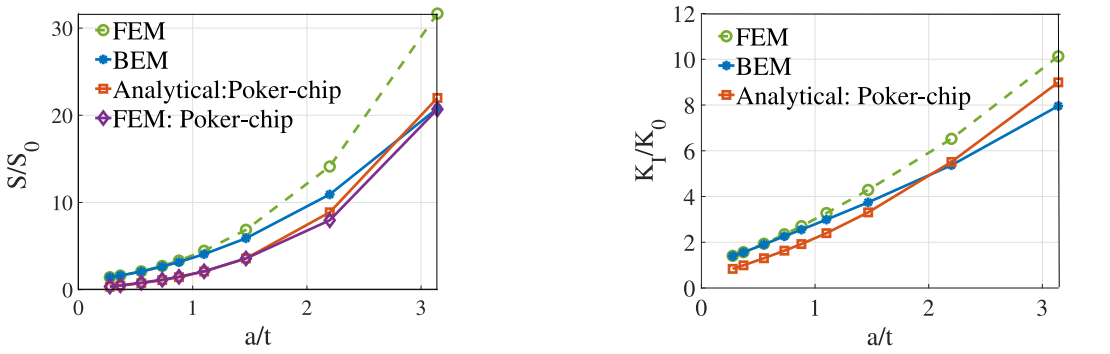

(a) Normalised contact stiffness (S/S_0) (b) Normalised Stress Intensity Factor (K_I/K_0)

Fig. 6. Moduli Mismatch ratio 1000:1, Poisson ratio $\nu_1 = 0.4999$, $\delta = 0.001$ mm, $a = 1.1$ mm while t is varying, Eq. (15).

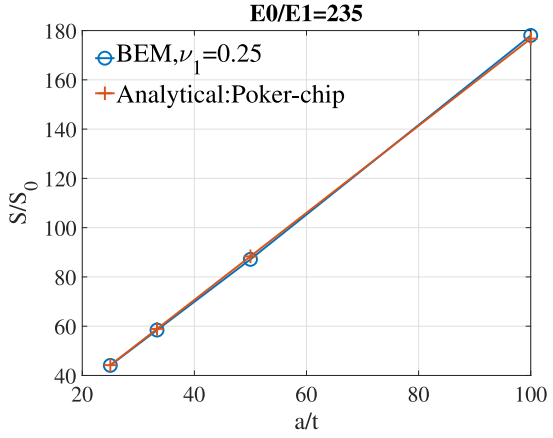

Fig. 7. Normalized contact stiffness (S/S_0), Moduli Mismatch ratio 235:1, Poisson ratio $\nu_1 = 0.25$, $\delta = 0.001$ mm, $a = 100$ mm while t is varying, Eq. (19).

the FEM result of the Poker-chip test is correct. The distinction is due to the boundary edge effect in the case of the FEM solution.

Moreover, when we employ Eq. (19) which is analytical solution of Pokerchip test when soft layer is compressible (i.e. $\nu_1 = 0.25$) and aspect ratios is very large (i.e. $a/t = 25, 33.33, 50, 100$), it agrees very well with corresponding BEM simulation as depicted in Fig. 7.

4. Conclusions

We analyzed linear models based on the Boundary Element Method (BEM), Finite Element Method (FEM), and the analytical Poker-chip test to evaluate contact stiffness and stress intensity factors for the flat punch contact problem in a coated elastic half-space. Our primary objective was to validate the semi-analytical BEM using FEM results and the analytical Poker-chip test, with a particular focus on both compressible and nearly incompressible soft layers.

The numerical algorithm based on BEM demonstrated robust performance for modulus mismatches (i.e. E_0/E_1) up to 100:1 and Poisson's ratios up to 0.4 within the studied aspect ratios. However, in the regimes characterized by extreme modulus mismatches and near-incompressible Poisson's ratios, BEM exhibited numerical challenges. To address these limitations, we employed analytical approaches such as the Poker-chip test, which provided reliable results in these parameter regimes. Hence, it is demonstrated that FEM simulations successfully captured the effects of incompressibility in confined soft layers, highlighting the limitations of BEM in handling highly incompressible materials. A critical remaining challenge is ensuring that BEM results align with full flat punch FEM simulations in these cases. Future work will focus on addressing the incompressibility issue in BEM.

CRediT authorship contribution statement

Krupal Patel: Writing – original draft, Visualization, Validation, Investigation, Formal analysis. **Etienne Barthel:** Writing – review & editing, Supervision, Project administration, Funding acquisition. **Matteo Ciccotti:** Writing – review & editing, Supervision, Project administration, Funding acquisition.

Declaration of competing interest

The authors declare that they have no known competing financial interests or personal relationships that could have appeared to influence the work reported in this paper.

Acknowledgments

"This project has received funding from the European Union's Horizon 2020 research and innovation program under the Marie Skłodowska-Curie grant agreement No 754387"

Appendix A

This code gives the value of stiffness and stress intensity factor in the case of conical indenter, flat-ended cylindrical punch, and spherical indenter indenting on the coated elastic half-space for the small strain limit.

```
# -*- coding: utf-8 -*-
"""
Created on 08/10/2020

@author: Krupal Patel & Rémy Brossard & Etienne Barthel
"""

from math import pi,exp,floor
import numpy as np
import matplotlib.pyplot as plt
import scipy.linalg as linalg
from numpy import linalg as LA
from decimal import Decimal
##############################################################################
#Indentation free parameter
##############################################################################
# contact radius
a=1.1
#Layer thickness
t=0.35
##############################################################################
#Tip parameters
##############################################################################
#Radius for the sphere or the flat punch
R=10
#tan(w) of the cone
tanw=2.8
##############################################################################
#Bilayer real parameters
##############################################################################
#Young's & Poisson's ratio of the half-space (Mpa)
E0=2950.81   #2900
v0=0.4754    #0.45
#Young's & Poisson's ratio of the layer (MPa)
E1=2.9999#2.999 #0.003
v1=0.4999#0.4999 # 0.5
##############################################################################
#Reduced Normalized variables
##############################################################################
tau=t/a
##############################################################################
#numeric
##############################################################################
#System size - typical 1000 - increase at large a/t
n=700
#FFT cut off B/2 and points number 2^vT
B=1000# this is cVmax in the original routine
vT=22
##############################################################################
#Tables
##############################################################################
G=np.array([0,1])
ZF=[]
M=np.eye(n)
V=np.array([0,1])
X=np.array([0,1])
#Fonction Z du papier
def GreenNormal(kt):
  gamma1=3-4*v1
  gamma3=3-4*v0
# difference HERE
```

```
  alpha=E1*(1+v0)/(E0*(1+v1))
  A=(alpha*gamma3-gamma1)/(1+alpha*gamma3)
  B=(alpha-1)/(alpha+gamma1)
  denominator=1-(A+B+4*B*(kt**2))*exp(-2*kt)+A*B*exp(-4*kt)
  C=(1+4*B*kt*exp(-2*kt)-A*B*exp(-4*kt))/denominator
  return C-1

#A smooth periodic approx
def makeZforFFT():
  global vMax
  vMax=float(B)/tau
  l=2**vT
  table=[1.2]*l

  dx=float(vMax)/(l-1)
  for i in range(int(l/2)):
    x=i*(dx)
    val=GreenNormal(x*tau)
    table[i]=val
    table[-i-1]=val
#  plt.plot([i*dx for i in range(l)], table)
  return table

#cosine transform
def makeTFC():
  global ZF
  Tinput=makeZforFFT()
  T_FFT=np.fft.rfft(Tinput)
  l=2**vT
#  print 1./l*vMax
  ZF=[x/2*vMax/l for x in T_FFT.real]
  #np.savetxt('result.txt',ZF)
#generates the coeficients of linear system
def generateMatrixTerms():
  global M
  makeTFC()
  bufferM=np.eye(n+1)
#  plt.figure("oh")
#  plt.plot([2*pi*y/vMax for y in range(len(ZF))],ZF)
  for i in range(n+1):
    for j in range(1,n):
      s=float(i)/n
      r=float(j)/n
      index_r_moins_s=abs(int((r-s)*vMax/(2*pi)))
      index_r_plus_s=abs(int((r+s)*vMax/(2*pi)))

    j=0
    s=float(i)/n
    r=float(j)/n
    index_r_moins_s=abs(int((r-s)*vMax/(2*pi)))
    index_r_plus_s=abs(int((r+s)*vMax/(2*pi)))
    bufferM[i,0]+=(ZF[index_r_moins_s]+ZF[index_r_plus_s])/(2*n*pi)
    #bufferM[i,0]/=1.

    if shape=='FLAT':
      j=n
      s=float(i)/n
      r=float(j)/n
      index_r_moins_s=abs(int((r-s)*vMax/(2*pi)))
      index_r_plus_s=abs(int((r+s)*vMax/(2*pi)))
      bufferM[i,n]+=(ZF[index_r_moins_s]+ZF[index_r_plus_s])/(2*n*pi)
      #bufferM[i,n]/=1
    else:
      bufferM[i,n]=-1.
  M=bufferM
```

```
#Right hand vector
def generateRightVector():
  global V
  Ar=[0]*(n+1)
  if shape==’CONIC’:
    for k in range(n+1):
      Ar[k]=-float(k)/n
  elif shape==’SPHERE’:
    for k in range(n+1):
      Ar[k]=-(float(k)/n)**2
  elif shape==’FLAT’:
    for k in range(n+1):
      Ar[k]=1
  V=Ar


#Let’s go!
def runFEBM():
  global X,G,DELTA,PI,delta,P,G_fp,S_fp
  print (shape,a,tau*a,R,tanw,E0,E1,v0,v1)
  CON=LA.cond(M)
  print(CON)
  generateMatrixTerms()
  generateRightVector()

 # X=np.linalg.solve(M,V)

  LU=linalg.lu_factor(M)

  X=linalg.lu_solve(LU,V)

  G=np.array([0.0]*(n+1))
  for k in range(n):
    G[k]=X[k]
  PI=4./n*np.sum(G)

  G_rho=X[n]

  if shape == ’CONIC’:
    delta=(pi/2)*(a/tanw)*G_rho  # penetration
    P=(pi/4)*(a**2*(E1/(1-v1**2))/tanw)*PI # force
    e_eq=PI/(2*G_rho**2)
    E_eq=E1*e_eq/(1-v1**2)
    print (G_rho,PI,delta,P,E_eq)
  elif shape==’SPHERE’:
    delta=(a**2/R)*G_rho # penetration
    P=0.5*(a**3*(E1/(1-v1**2))/R)*PI # force
    e_eq=(3./8.)*PI/(G_rho**(1.5))
    E_eq=E1*e_eq/(1-v1**2)
    print (G_rho,PI,delta,P,E_eq)
  elif shape==’FLAT’:
    delta=0.001
    #G_fp=(G_rho*2*(1-v1**2))/(E1*delta)
    G_fp=(G_rho*E1*delta)/((1-v1**2)*(np.pi*a)**(1/2))  # Stress Intensity
    #G_fp=(delta*E1)/((1-v1**2)*(2*(2*np.pi*a)**(1/2)))

    S_fp=PI*E1/(1-v1**2)/2*a# stiffness
    e_eq=PI/4.
    E_eq=E1*e_eq/(1-v1**2)

    print (G_rho,delta,PI/4.0,G_fp,S_fp)

# shape=’CONIC’
# runFEBM()
# shape=’SPHERE’
# runFEBM()
shape=’FLAT’
runFEBM()
```

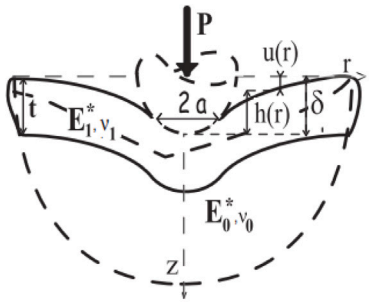

Fig. B.1. Contact geometry for a thin film.

Table B.1
BEM code nomenclature.

Code manual	
Variable name	Nomenclature in the Python code
Contact radius	a
Thickness of the layer	t
Radius for the sphere	R
Cone angle	w
Normalized thickness	τ
Young's modulus of the half-space and Poisson's ratio of the half-space	E_0 and ν_0
Young's modulus of the layer and Poisson's ratio of the layer	E_1 and ν_1
System size	n
FFT Cut off	B
The number of points in the fourier space	υ_T
An array related to the response function $C(kt)$ after cosine transform	ZF
An array related to the response function $C(kt)$	M
An array related to the right hand side of the system AX=B	V
An array pertaining to the solution of the system AX=B	X
Stiffness in N/mm	S_{fp}
Stress Intensity factor in MPa $mm^{1/2}$ of the flat punch indentation	G_{fp}
Normalized force and Displacement in mm for the cone and sphere indentation	PI and δ
Surface stress transform	Γ

Appendix B

In Appendix A, the Python routine is given. Here, we explain how to use the code and its numerical implementation. First, we imported the main Python libraries needed which are as follow: (1) math, (2) numpy, (3) matplotlib.pyplot, (4) scipy.linalg. We give the explanation of variable names of Python code in the Table B.1.

B.1. Coated substrates – thin films

A schematic representation of the indentation of a coated elastic half-space is given in Fig. B.1

B.2. Normalized solution

The procedure to compute a full-force curve for the adhesive contact for a given value of the contact radius, a is as follows:

1. compute the adhesionless penetration and force for the given indenter shape
2. compute the force and stress intensity factor (or $g(a)$) for the flat punch for a unit value of the penetration

Table B.2
Transformation applied to variables in BEM due to normalization.

Variable	Cone	Sphere	Flat punch
Δ	$\frac{2}{\pi}\frac{\tan(\beta)}{a}\delta$	$\frac{R}{a^2}\delta$	$\delta/\delta = 1$
$\Theta(\rho)$	$\Delta - \rho$	$\Delta - \rho^2$	Δ
$G(\rho)$	$\frac{2}{\pi}\frac{\tan(\beta)}{aE_1^*}g(r)$	$\frac{3R}{4a^2E_1^*}g(r)$	$\frac{2}{\delta E_1^*}g(r)$
Π	$\frac{2}{\pi}\frac{\tan(\beta)}{a^2E_1^*}P$	$\frac{3R}{4a^3E_1^*}P$	$P/\delta = 4\mathcal{E}_{\text{eq}}^*$

3. compute actual value of $g(a)$ from Eq. (12) and re-scale flat punch force and penetration
4. compute the solution from Eq. (13) which we got after applying mixed boundary conditions.

This provides the solution in the form of two relations between the local deformation (stress intensity factor) and the local response on the one hand and the remote loading and the macroscopic response (contact stiffness) on the other hand.

In the normalized form, with

$$\tilde{r} = \frac{r}{t} \tag{B.1}$$

one has[1]

$$F_{0,s} = \frac{4a^3 {E_1}^\star}{3R}\Pi_s(\tilde{a}, t, [E]) \tag{B.2}$$

$$\delta_{0,s} = \frac{a^2}{R}\Delta_s(\tilde{a}, t, [E]) \tag{B.3}$$

$$S = 2a{E_1}^\star \mathcal{E}_{\text{eq}}(\tilde{a}, t, [E]) \tag{B.4}$$

$$g(r; a, t, [E]) = \frac{\delta_{fp}{E_1}^\star}{2}\Gamma(\tilde{r}; \tilde{a}, t, [E]) \tag{B.5}$$

where the normalized variables can be numerically calculated by the simple algorithm presented in [30]. Following [30], we introduce the following normalized quantities

$$\rho \equiv \frac{r}{a};\ \tau \equiv \frac{t}{a};\ \eta \equiv ka \tag{B.6}$$

For the homogeneous substrate, all normalized variables equal 1. $\Gamma(\tilde{r}; \tilde{a}, t, [E])$ is the surface stress transform normalized to penetration δ. In particular, $\Gamma(\tilde{a}; \tilde{a}, t, [E])$, denoted $\Gamma(1)$ below for brevity, is the contact edge singularity $g(a; a, t, [E])$ incurred for a coated system – normalized to a homogeneous material with the film elastic properties – at identical δ_{fp} value. The variable $\Gamma(1)$, which is positive since both δ_{fp} and $g(a)$ are negative in Eq. (B.5), is a function of $\tilde{a}$, and depends upon the mechanical parameters of the system.

In the case of a homogeneous material, a combination of Eqs. (12), (10) and (11) allows us to solve the problem easily. In principle, similar auxiliary functions can be built to diagonalize Eq. (13) for the coated system. In practice, as explicit expressions have not been obtained yet, we introduced a numerical method to invert Eq. (13).

B.3. Problem definition

Let us now consider Eq. (13) for application to an indentation experiment. Let us not make any hypothesis on the shape of the indenter, apart from the fact that it is rigid, convex, axisymmetric, and frictionless. For simplicity, we will consider the contact between the indenter and the coated material to be non-adhesive. The boundary conditions of this problem are the following :

$$\begin{cases} \forall r \le a, & u(r) = \delta - h(r) \\ \forall r \ge a, & q(r) = 0 \end{cases} \tag{B.7}$$

where $h(r)$ the shape of the indenter and a the contact radius.

Note that this type of loading, because it only considers the normal displacement, does not model the indenter shape exactly, as has been shown by Hay et al. [31]. The minor corrections taking into account the radial displacement will not be considered here.

Combining Eqs. (10) and (B.7), we have :

$$\forall\, r \ge a, g(r) = 0 \tag{B.8}$$

Eq. (13) then becomes :

$$\theta(s) = \frac{2}{\pi}\int_0^a g(r)\left(\int_0^\infty dk\, C(k)\cos(kr)\cos(ks)\right)dr \tag{B.9}$$

[1] For a cone:

$$F_{0,c} = \frac{\pi a^2 {E_1}^\star}{2\tan\beta}\Pi_c(\tilde{a}, t, [E])$$

$$\delta_{0,c} = \frac{\pi a}{2\tan\beta}\Delta_c(\tilde{a}, t, [E])$$

while $\theta(r)$ is known on $[0;a]$ through Eqs. (11) and (B.7). Then, under the contact, our indentation problem turns into an integral equation of the type $h(r) = \int_0^a ds f(s)K(r,s)$ where h and K are known.

As the method is similar to whatever the indenter shape, we will only detail here the calculation in the case of the cone indentation. Introducing,

$$\mathcal{Z}(x) \equiv \frac{\alpha E_1^*}{2} C(x) - 1 \tag{B.10}$$

$$\Theta(\varsigma) = G(\varsigma) + \frac{2}{\pi}\int_0^1 G(\rho)\left(\int_0^\infty d\eta\, \mathcal{Z}(\eta\tau)\cos(\eta\rho)\cos(\eta\varsigma)\right) d\rho \tag{B.11}$$

from which Δ and G can be calculated and

$$\Pi = 4\int_0^1 d\rho\, G(\rho) \tag{B.12}$$

Here the normalization parameter α is $\alpha_{fp} = 1$ for the flat punch, $\alpha_{cone} = 2$ for the cone and $\alpha_{sphere} = 8/3$ for the sphere. With

$$\epsilon = \frac{u(a)}{\frac{P}{S}} \tag{B.13}$$

we have for the cone:

$$\epsilon = 4\frac{\Delta - \frac{2}{\pi}}{\frac{\Pi}{E_{eq}}} \tag{B.14}$$

and for the sphere:

$$\epsilon = 4\frac{\Delta - \frac{1}{2}}{\frac{\Pi}{E_{eq}}} \tag{B.15}$$

B.4. Implementation of the model

Let us consider Eq. (B.11) and discretize $[0;1]$ into N. From now on, we shall use $\varsigma_i = i/N$ and $\rho_j = j/N$. If we approximate the integral on ρ by a discrete sum, we then get :

$$\begin{aligned}\Delta - \varsigma_i = G(\varsigma_i) &+ \frac{1}{N\pi}G(0)K(\varsigma_i,0,\tau) + \frac{1}{N\pi}G(1)K(\varsigma_i,1,\tau)\\ &+ \frac{2}{N\pi}\sum_{j=1..N-1} G(\rho_j)K(\varsigma_i,\rho_j,\tau)\end{aligned} \tag{B.16}$$

with $K(\varsigma,\rho,\tau) = \int_0^\infty d\eta\, \mathcal{Z}(\eta\tau)\cos(\eta\rho)\cos(\eta\varsigma)$

From Eq. (B.11) we have $G(1) = 0$. Then, for a given τ – that is to say for a given contact radius – we have to solve the $(N+1)\times(N+1)$ linear system introduced in Eq. (B.16) for the remaining N values of the G field and the normalized penetration Δ. The $\underline{\underline{K}}$-matrix elements can be calculated with a Fast Fourier Transform (FFT) algorithm for numerical efficiency. Finally, the applied load Π and equivalent modulus $\mathcal{E}_{eq}^*$ are obtained through Eq. (B.12) and Table B.2

B.5. Numerical considerations

The accuracy of the numerical solution depends on the dimension N of the $\underline{\underline{K}}$ matrix (which is associated to the discretization of $[0;1]$), the cut-off B for the sampling range of the $\mathcal{Z}$ function and the sampling rate $B/2^k$ for the FFT calculation of the matrix elements.

As $\mathcal{Z}$ decreases in an exponential-like way and tends to zero when η becomes infinite, it is possible to choose a rather small value for B. We first considered the case $a/t = 100$ and chose $B = 1000$. We then tested increasing values of N and k. Our results appear to converge with a deviation smaller than 1% when N is greater than 700 (for a given k of 19) and when k is greater than 14 (with $N = 700$).

However, with $N = 700$ and $B = 1000$, the output returned for small values of a/t converges only for $k = 20$, as the decay length of $\mathcal{Z}$ decreases with a/t. This leads to an increase in terms of calculation time. Thus, we decided to fix $N = 700$ and $k = 14$, which constitutes a good compromise between calculation time and precision, and to adapt the value for B to the input value for a/t. For instance, for $a/t < 1$, $B = 20$ is sufficient as $\mathcal{Z}(20)/\mathcal{Z}(0)$ is smaller than 10^{-14} for moduli ratios up to 100.

For numerical calculations, it is necessary to select adequate value of the parameters n, B, V_T. The convergence has been studied for getting the correct results out of BEM. Especially the impact of the parameters n, B, V_T for flat punch contact to the coated substrate is studied in Figs. B.2(a)–B.2(c). As the value of n, B, and V_T increases, the value of contact stiffness converges for modulus contrast 100 and layer Poisson's ratio 0.4. It is found that values of $n = 700$, $B = 1000$ and $V_T = 20$ are adequate to find the correct value of the contact stiffness as there is not much change in the value of contact stiffness by further increasing these parameters.

Appendix C

Here, we explain how the response function or Green's function becomes singular for elevated confinement and Poisson's ratio approaching 0.5.

Using the notation

$$C(kt) = \frac{2}{E_1{}^*}\frac{N}{D} \tag{C.1}$$

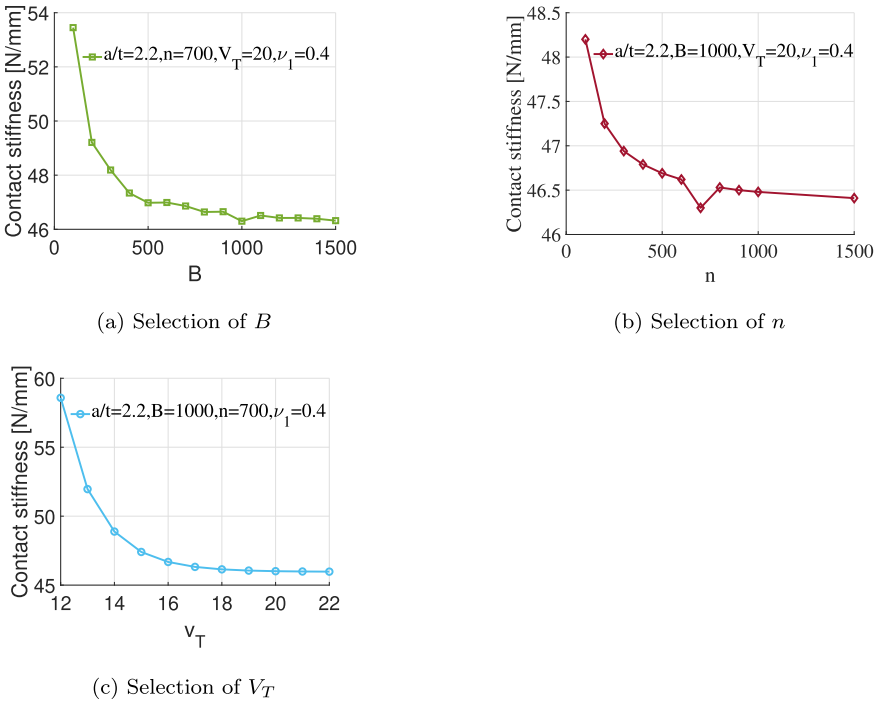

(a) Selection of B (b) Selection of n

(c) Selection of V_T

Fig. B.2. Convergence study using parameters (a) B, (b) n, (c) V_T for the case of $a/t = 2.2$, $E_0/E_1 = 100$ and $\nu_1 = 0.4$.

Since we are interested in the highly confined limit, we will look at the large aspect ratios (i.e. the small k values, where k is the wave vector in the Fourier space). Expanding at small kt, we find that the numerator is given by

$$\begin{aligned} N &= 1 + 4b\,kt\left[1 + \frac{-2kt}{1!} + \frac{4k^2t^2}{2!} + \cdots\right] \\ &\quad -ab\left[1 + \frac{-4kt}{1!} + \frac{16k^2t^2}{2!} - \frac{64k^3t^3}{3!} + \cdots\right] \\ &= (1-ab) + (kt)(4b+4ab) + (kt)^2(-8b-8ab) \\ &\quad +(kt)^3(8b + ab\frac{32}{3}) + \cdots \end{aligned} \tag{C.2}$$

The denominator is given by

$$\begin{aligned} D &= 1 - (a+b+4b(kt)^2)\left[1 + \frac{-2kt}{1!} + \frac{4k^2t^2}{2!}...\right] \\ &\quad +ab\left[1 + \frac{-4kt}{1!} + \frac{16k^2t^2}{2!} - \frac{64k^3t^3}{3!} + \cdots\right] \\ &= (1-a-b+ab) + (kt)(2a+2b-4ab) + (kt)^2(-2a-6b+8ab) \\ &\quad +(kt)^3(8b - ab\frac{32}{3}) + \cdots \end{aligned} \tag{C.3}$$

From the expression of the $C(kt)$ given in Eq. (5), it can be seen that as k goes to zero, E_0 goes to infinity and ν_1 goes to 0.5 then

$$\alpha = 0, a = -1, b = -1. \tag{C.4}$$

We see that D is well-behaved but the first three terms in the expansion of the N go to zero. This is the direct consequence of a confined incompressible soft layer. This is the probable source of the problem with the BEM method in this regime.

In fact, at finite thickness t and large radius a, (i.e. taking the limit kt goes to zero), we recover from Eq. (5), the uniaxial strain compliance $C = \frac{(1+\nu_1)(1-2\nu_1)}{E_1(1-\nu_1)}$. It duly goes to zero when the material becomes incompressible. This is an effect of confinement. Hence, the apparent reason for the breakdown of the BEM method at a high aspect ratio and the incompressible coating layer is visible here.

Data availability

Code is available in the article itself.

References

[1] Vasinonta A, Beuth JL. Measurement of interfacial toughness in thermal barrier coating systems by indentation. Eng Fract Mech 2001;68(7):843–60, CrossRef.

[2] Bolzon G, Buljak V, Maier G, Miller B. Assessment of elastic–plastic material parameters comparatively by three procedures based on indentation test and inverse analysis. Inverse Probl Sci Eng 2011;19(6):815–37, CrossRef.

[3] Hodzic A, Kalyanasundaram S, Kim JK, Lowe AE, Stachurski ZH. Application of nano-indentation, nano-scratch and single fibre tests in investigation of interphases in composite materials. Micron 2001;32(8):765–75, CrossRef.

[4] Iqbal HMS, Bhowmik S, Benedictus R. Performance evaluation of polybenzimidazole coating for aerospace application. Prog Org Coat 2017;105:190–9, CrossRef.

[5] Sneddon IN. The relation between load and penetration in the axisymmetric boussinesq problem for a punch of arbitrary profile. Internat J Engrg Sci 1965;3:47–57, CrossRef.

[6] Jaffar MJ. A numerical solution for axisymmetric contact problems involving rigid indenters on elastic layers. J Mech Phys Solids 1988;36(4):401–16, CrossRef.

[7] Jaffar MJ. Frictionless contact between an elastic layer on a rigid base and a circular flat-ended punch with rounded edge or a conical punch with rounded tip. Int J Mech Sci 2002;44(3):545–60, CrossRef.

[8] Yang F. Indentation of an incompressible elastic film. Mech Mater 1998;30(4):275–86, CrossRef.

[9] Hayes WC, Keer LM, Herrmann G, Mockros LF. A mathematical analysis for indentation tests of articular cartilage. J Biomech 1972;5(5):541–51, CrossRef.

[10] Lebedev NN, Ufliand IaS. Axisymmetric contact problem for an elastic layer. J Appl Math Mech 1958;22(3):442–50, CrossRef.

[11] Xu Z-H, Rowcliffe D. Finite element analysis of substrate effects on indentation behaviour of thin films. Thin Solid Films 2004;447:399–405, CrossRef.

[12] Sun Y, Bloyce A, Bell T. Finite element analysis of plastic deformation of various TiN coating/substrate systems under normal contact with a rigid sphere. Thin Solid Films 1995;271(1–2):122–31, CrossRef.

[13] Lee C-C, Lin Y-F, Liou Y-Y, Huang P-C, Liang C-C, Yeh S-T, Chen H-Y. Simulated and experimental demonstrations of interfacial adhesive strength for released layer utilized in flexible electronics. Thin Solid Films 2020;706:138022, CrossRef.

[14] Djabella H, Arnell RD. Finite element analysis of contact stresses in elastic double-layer systems under normal load. Thin Solid Films 1993;223(1):98–108, CrossRef.

[15] Zak S, Trost C, Kreiml P, Cordill MJ. Accurate measurement of thin film mechanical properties using nanoindentation. J Mater Res 2022;37(7):1373–89, CrossRef.

[16] Lassnig A, Zak S. Precise determination of Young's modulus of amorphous CuZr/nanocrystalline Cu multilayer via nanoindentation. J Mater Res 2023;38(13):3324–35, CrossRef.

[17] Zak S. Controlling strain localization in thin films with nanoindenter tip sharpness. Sci Rep 2024;14(1):25500, CrossRef.

[18] Li Q, Pohrt R, Lyashenko IA, Popov VL. Boundary element method for nonadhesive and adhesive contacts of a coated elastic half-space. Proc Inst Mech Eng Part J: J Eng Tribol 2020;234(1):73–83, CrossRef.

[19] Boussinesq J. Applications des potentiels à l'étude de l'équilibre et du mouvement des solides éstiques. Gauthier- Villars; 1885, CrossRef.

[20] Love AEH. Boussinesq's problem for a rigid cone. Q J Math 1939;10:161–75, CrossRef.

[21] Love AEH. IX. The stress produced by semi-infinite solid by pressure on part of boundary. Phil Trans R Soc A 1929;228:377–420, CrossRef.

[22] Li J, Chou T-W. Elastic field of a thin-film/substrate system under an axisymmetric loading. Int J Solids Struct 1997;34:4463–78, CrossRef.

[23] Huajian G, Cheng-Hsin C, Jin L. Elastic contact versus indentation modeling of multi-layered materials. Int J Solids Struct 1992;29:2471–92, CrossRef.

[24] Huguet A-S, Barthel E. Surface forces and the adhesive contact of axisymmetric elastic bodies. J Adhes 1999;74:143–75, CrossRef.

[25] Barthel E, Perriot A, Chateauminois A, Frétigny C. Elastic contact to nearly incompressible coatings - Stiffness enhancement and elastic pile-up. Philos Mag Taylor Fr 2006;86:5359–69, CrossRef.

[26] Perriot A, Barthel E. Elastic contact to a coated half-space - Effective elastic modulus and real penetration. J Mater Res 2004;19:600–8, CrossRef.

[27] Lin YY, Hui C-Y, Conway HD. A detailed elastic analysis of the flat punch (tack) test for pressure-sensitive adhesives. J Polym Sci Part B: Polym Phys 2000;38(21):2769–84, CrossRef.

[28] Barthel E. Adhesive elastic contacts: JKR and more. J Phys D: Appl Phys 2008;41:163001–21, CrossRef.

[29] Sussman T, Bathe KJ. A finite element formulation for nonlinear incompressible elastic and inelastic analysis. J Comput Struct 1987;26:357–409, CrossRef.

[30] Haiat G, Barthel E. Approximate model for the adhesive contact of viscoelastic spheres. Langmuir 2002;18:9362–70, CrossRef.

[31] Hay JC, Bolshakov A, Pharr GM. A critical examination of the fundamental relations used in the analysis of nanoindentation data. J Mater Res 1999;14:2296–305, CrossRef.